JOURNAL OF PROPULSION AND POWER
Vol. 16, No. 2, March–April 2000

Numerical Thermal Model of NASA Solar Electric Propulsion Technology Application Readiness Ion Thruster

Jonathan Van Noord* and Alec Gallimore†
University of Michigan, Ann Arbor, Michigan 48109-2140
and
Vincent K. Rawlin‡
John H. Glenn Research Center at Lewis Field, Cleveland, Ohio 44135

A thermal computer model of the 30-cm NASA solar electric propulsion technology application readiness (NSTAR) xenon ion thruster has been produced using a lumped-parameter thermal nodal-network scheme. This model contains 104 nodes on the thruster and was implemented using SINDA and TRASYS on various UNIX workstations. The model includes the radiation and conduction heat transfer, the effect of plasma interaction on the thruster, and an account for finely perforated surfaces. The model was developed in conjunction with an NSTAR thruster outfitted with approximately 20 thermocouples for thermal testing at the John H. Glenn Research Center. The results of these experiments were used to calibrate and confirm the computer model first without and then with the plasma interaction. The calibrated model was able to predict discharge chamber temperatures to within 10°C of measured temperatures. To demonstrate the ability of the model under various circumstances, the heat flux was examined for a thruster operating in a deep-space environment.

Nomenclature

A_I = area of Ith element, m^2
A_J = area of Jth element, m^2
C_i = thermal capacitance at node i, cal/g · K
F_{ij} = form (view) factor
G_{ji} = linear conductor attaching node j to node i, W/K
H_{ji} = radiation conductor attaching node j to node i, W/K^4
J_A = ion current hitting grid, A
J_B = ion beam current, A
N = number of nodes
Q_i = heat source or sink for node i, W
r_{ij} = distance between the ith and jth element, m
T_i^{k+1} = temperature of node i for the $k+1$ iteration, K
T_i^{n+1} = temperature of node i at time $t + \Delta t$, K
T_i^k = temperature of node j for the kth iteration, K
T_n^j = temperature of node j at time t, K
U_+^j = ionization energy, eV
V_P = discharge chamber plasma potential with respect to ambient space plasma potential, V
θ_i = angle between normal of ith element and the line connecting the ith and jth element, rad
θ_j = angle between normal of jth element and the line connecting the ith and jth element, rad
Φ_N = neutralizer power, W
Φ_{sh} = self-heating power deposited in the discharge chamber in the form of heat, W
Φ_T = total thruster power, W

I. Introduction

THE 30-cm-diam ring cusp ion thruster produced from the NASA Solar Electric Propulsion Technology Application Readiness (NSTAR) program represents the state of the art in ion thruster technology. Ion thrusters have long been known to have the highest efficiency at high specific impulse of all electric propulsion devices. The combination of high power-utilization efficiency at specific impulses in excess of 3000 s has made the ion engine an attractive candidate for high-delta-V planetary missions.

Despite these advantages, however, application of ion propulsion to scientific, military, and commercial spacecraft was hampered in the past by perceived high engine development costs and the inability of spacecraft manufacturers to reliably identify potential integration and thruster lifetime issues. The primary concerns that spacecraft manufacturers had in regard to using ion propulsion included the likely impact of thruster operation on spacecraft design and operations, electromagnetic compatibility, spacecraft contamination from thruster efflux, spacecraft damage from the plume, thruster reliability, and thermal loading of the spacecraft from the thruster. Ion propulsion became (and will continue to become) more attractive once tools were developed, e.g., plume PIC codes,[1] which helped spacecraft manufacturers identify potential spacecraft integration issues associated with this technology.

One of the key objectives of NASA's first new millennium mission, Deep Space 1, is to evaluate and validate the 30-cm NSTAR ion thruster. Launched in October 1998, Deep Space 1 is slated to fly by an asteroid and comet in 1999. A slightly more advanced version of this thruster is slated for the 2003 Deep Space 4 mission, which will land a spacecraft on the nucleus of a comet.[2]

Given the wide range of thermal environments an ion thruster on a deep-space mission will likely encounter, it is essential that computer tools be developed to predict the temperatures of thruster components over the expected range of operating and thermal conditions. Some critical areas of concern include the degaussing of permanent magnets from excess heating, freezing of xenon in propellant lines,[3] distortion of the ion optics from thermal gradients,[4] and spacecraft integration issues in general, e.g., thermal soakback. Although work has been done in the past to model the thermal behavior of 20-cm-diam (Ref. 5) and 30-cm-diam (Ref. 6) divergent-field ion thrusters utilizing mercury propellant, no such model has been developed for modern ring cusp xenon thrusters such as the NSTAR engine. The most recent approaches used to develop the thermal models started with analytical models to determine thruster self-heating from the plasma but then relied on data from experiments to adjust the numerical model to fit measured thruster temperatures. This same approach was used to determine the self-heating terms on

Received 12 December 1997; revision received 11 March 1999; accepted for publication 29 March 1999.

*Graduate Student Research Assistant, Department of Aerospace Engineering, 1320 Beal Avenue. Member AIAA.
†Associate Professor, Department of Aerospace Engineering, 1320 Beal Avenue. Associate Fellow AIAA.
‡Aerospace Engineer, Onboard Propulsion Branch, 21000 Brookpark Road. Member AIAA.

the NSTAR thruster. The tests used for calibrating this model were based on experiments performed at John H. Glenn Research Center in June and July 1996.

Once adjusted to match experiments, the model can then be used to investigate other operating conditions. It has already been used to alert of the possible dangers of overheating the magnets at certain thruster settings. Other issues investigated but not presented here include enclosing the thruster in an adiabatic surface, changing materials on the thruster, and determining the influence of ambient conditions in space on the thruster.

II. Model Description

A. Thermal Model

There are two major modes of heat transfer that take place in the NSTAR thruster. The dominant process is radiation heat transfer,[6] but conduction still plays a major role in establishing thruster component temperatures. The interaction of the plasma with the thruster will be discussed later. To handle a model of significant size and to study the thermal response of the thruster to various steady-state and periodic external radiation loads over its full range of operating conditions, a computer model was utilized using two well-used codes.

SINDA analyzes thermal systems represented in electrical analogy, lumped parameter form.[7] The conductors based on the conductive and radiative properties of the system are calculated between nodes and then are included in the SINDA input file. The equation used for steady-state analysis in SINDA is

$$0 = Q_i + \sum_{j=1}^{i-1}\left[G_{ji}\left(T_j^{k+1} - T_i^{k+1}\right) + H_{ji}\left\{\left(T_j^{k+1}\right)^4 - \left(T_i^{k+1}\right)^4\right\}\right] + \sum_{j=1}^{N}\left[G_{ji}\left(T_j^{k} - T_i^{k+1}\right) + H_{ji}\left\{\left(T_j^{k}\right)^4 - \left(T_i^{k+1}\right)^4\right\}\right] \tag{1}$$

which is solved by a successive point iterative method.[7] The transient equation used is based on an implicit forward–backward differencing method,

$$\frac{2C_i}{\Delta t}\left(T_i^{n+1} - T_i^{n}\right) = 2Q_i + \sum_{j=1}^{N}\left[G_{ji}\left(T_j^{n} - T_i^{n}\right) + H_{ji}\left\{\left(T_j^{n}\right)^4 - \left(T_i^{n}\right)^4\right\}\right] + \sum_{j=1}^{N}\left[G_{ji}\left(T_j^{n+1} - T_i^{n+1}\right) + H_{ji}\left\{\left(T_j^{n+1}\right)^4 - \left(T_i^{n+1}\right)^4\right\}\right] \tag{2}$$

For Eqs. (1) and (2) the radiation terms are linearized before solution routines are initiated.

The second piece of software used is TRASYS.[8] TRASYS uses geometry and surface characteristics to provide radiation conductors for SINDA. TRASYS computes the radiation view factors using the Nusselt sphere and double summation techniques.[8] Both of these calculation methods are based on the equation

$$F_{ij} = \int_{A_I}\int_{A_J} \frac{\cos\theta_i \cos\theta_j}{\pi r_{ij}^2}\, dA_J\, dA_I \tag{3}$$

which gives the view factor for two finite areas.

Typically in thermal analysis, test-calibrated models are given an 11°C margin wherein 95% of the temperatures are expected to fall.[9] SINDA has been shown to match an analytical solution of a very simple, warm body radiatively cooled to a heat sink to within 1°C (which was an absolute error of less than 0.5%).[10] However, more complex models will have a higher degree of uncertainty. Contact resistance is a common reason for the uncertainty. Meshed or perforated surfaces are also known to be extremely difficult to analyze. This is due to the complex shadowing involved when one surface interacts with another through the meshed surface and also due to the complex radiation interchange between all of these surfaces.[9] The ground screen (screen around the thruster body, which NSTAR nomenclature lists as the plasma screen) temperatures on Oglebay's[6] SINDA model differed up to 33°C from experimental values. Because the accuracy of a model is dependent on its complexity, a thermal model is often a balance between being too complex, which takes significant modeling and computing time and can result in confusion when interpreting the results, to being too simple and not very accurate.

The NSTAR model contains 104 thruster nodes with conductors connecting the nodes for conduction and radiation heat transfer. The thruster is essentially broken up into four quadrants. Two of the quadrants are further subdivided in half to accommodate the gimbal pads. It is the presence of gimbal pads and the neutralizer that prevents the thruster from being modeled as a pure symmetrical body. If it were purely symmetrical, the thruster would only vary in temperature along the axis and not circumferentially. Dividing the thruster into four main quadrants with two of them subdivided for the gimbal pads is the simplest form of modeling, which uses the symmetrical nature it does have while accounting for the unsymmetrical elements. Because the neutralizer has been shown to be insignificant in its thermal impact to the thruster,[6] a simplified neutralizer model was used. Figure 1 shows the nodal layout of the thruster. The nodal numbering scheme in Fig. 1 for off-axis nodes starts with the lowest number on the bottom (in the quadrant of the neutralizer) and then increases by one for each quadrant in a counterclockwise manner when viewed from the optics end of the thruster. This scheme is true for all of the nodes except those on the neutralizer (nodes in the 400s), which are contained only in the one quadrant, and the discharge cathode (nodes 1–13), which is divided in half. The discharge cathode and keeper nodes are shown in Fig. 2.

The tests that were used to calibrate the NSTAR model took place at the John H. Glenn Research Center.[11] There were two different types of experiments modeled. The first was a cold-soak experiment to subject the thruster to the severe cold conditions of space without any heat source from its operation, and the second type was the same cold conditions, but with heat present from its operation. The experimental setup at John H. Glenn Research Center included

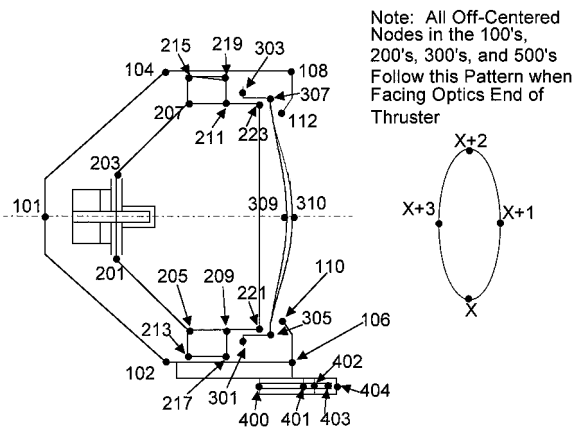

Fig. 1 NSTAR ion thruster thermal model nodal layout.

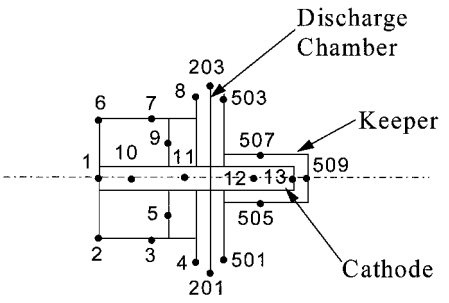

Fig. 2 NSTAR cathode thermal model layout.

the thruster enclosed within a 116-cm-diam liquid-nitrogen-coded shroud contained in a 4.6-m-diam × 19.5-m-long vacuum chamber. Figure 3 shows the setup of the shroud in the vacuum chamber. The tubes carrying the liquid nitrogen snaked circumferentially around the outside of the shroud. The open end of the shroud was closed off by a door, which did not have any direct contact with the liquid nitrogen, but was painted black on the inside and cooled by the rest of the shroud through radiation. In the experiment used for the steady-state analysis, the rear of the shroud was cooled with liquid nitrogen, but not in the transient case. A ring piece was located close to the front (optics end) of the thruster face and was cooled through conduction with the cylindrical part of the shroud. It was used to minimize the interaction between the thruster and the vacuum chamber wall. The shroud was made of stainless steel and painted with a commercial, high-temperature, fireplace flat black paint with a measured emissivity of 0.9.

The model used temperature measurements along the shroud and tank walls to establish boundary conditions. These boundary nodes consisted of 37 nodes making up the shroud and experimental setup and 6 nodes for the tank wall. There were several thermocouples used to establish these boundary conditions. The vacuum tank had two thermocouples placed on opposite sides of the wall's circumference and about halfway from each end. The main thermocouples used on the shroud are shown in Fig. 4, which also shows the surfaces used in the TRASYS form factor analysis. The thermocouples were mostly type K with a few type R for higher temperature regions. Type K are rated with an accuracy of 2.2°C or 0.75% and type R are rated with an accuracy of 1.5°C or 0.25%. The larger value will determine the accuracy, and so for most of the thruster thermocouples, the accuracy will be between 2 and 5°C. The thermocouples that were on the outside of the discharge chamber were attached magnetically, and the rest were spot-welded. Tests were performed earlier on grounded thermocouples with and without covers and revealed no temperature difference from the plasma. All of the thermocouples, except for the one on the cathode keeper, were on the outside of the discharge chamber and away from the dense plasma. Most were inside the plasma screen and, therefore, away from the low-density, low-energy vacuum tank plasma. The thruster was modeled as being isolated from the shroud and its test stand. The model does not include the feed lines, the electrical lines, or the isolator box because those are predicted to have minimal impact on the thermal characteristics of the thruster. Figure 5 shows these components and others that make up the thruster.

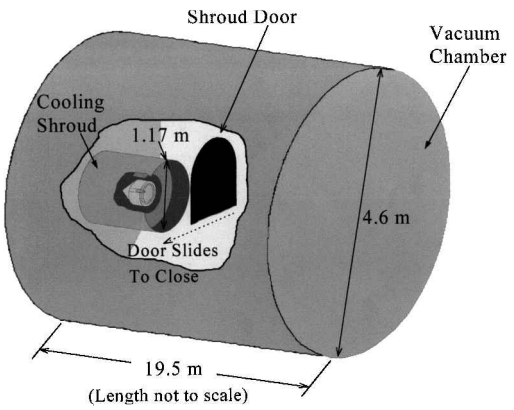

Fig. 3 Experimental setup of cooling shroud in vacuum tank.

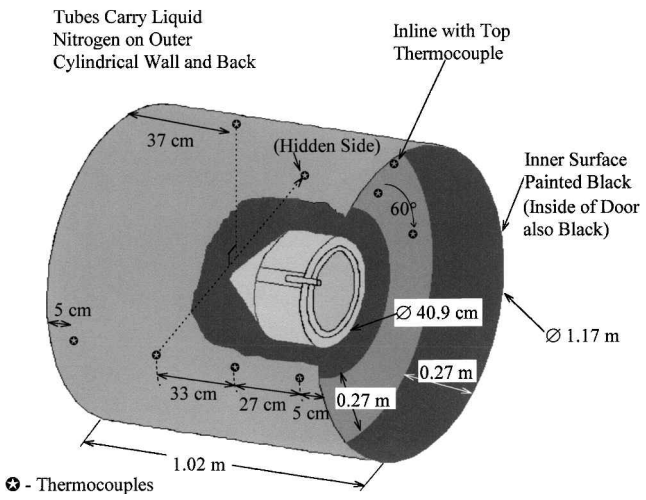

Fig. 4 Model layout of thruster in cooling shroud.

Table 1 Assumed physical properties of ion thruster materials

Material	Density, g/cm^3	Heat capacity cal/g °C	Conductivity, W/cm °C	Emissivity
Aluminum 5052	2.68	0.20	1.37	0.14 0.30[a]
Pure titanium	4.43	0.15	0.2	0.23 0.4[a]
Carbon steel	7.81	0.13	0.60	Not needed
304 Stainless	7.92	0.125	0.20	0.11 0.27[a] 0.5[b]
Molybdenum	10.19	0.20	1.20	0.2
Tantalum	16.16	0.035	0.60	0.1
Tungsten	19.38	0.035	1.50	0.1
Alumina	3.79	0.20	0.17	0.3
Kovar	8.36	0.105	0.15	0.1
6Al-4V titanium	4.43	0.15	0.10	0.15

[a]Grit-blasted surface. [b]Meshed surface.

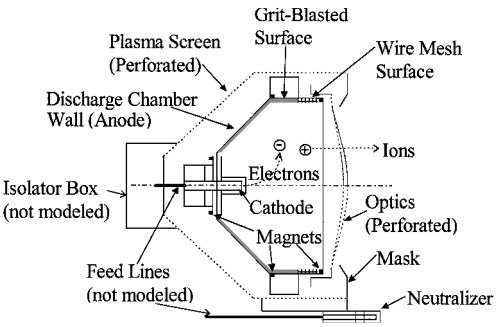

Fig. 5 NSTAR thruster layout.

Because radiation is the major form of heat transfer within the thruster, accurate surface property values are very important. Changing materials or surface properties could modify the thermal characteristics of the thruster significantly. These properties could also change over the life of the thruster further complicating matters. For this model the emissivities of materials were assumed to be constant throughout the temperature range examined, which is a valid assumption for the conditions experienced by the thruster. Emissivities in the infrared surface temperature regime were obtained from published sources and also from experiments conducted with components of the NSTAR thruster (Table 1).[3,12–14] Emissivities that could not be determined used Oglebay's[6] values of 0.1. Joint (contact) conductances were modeled with a constant conductivity of 0.0057 W/cm^2 °C on the basis of experiments.[6] All other material properties used in the model are listed in Table 1. The grit-blasted surfaces referred to in Table 1 are on the inside of the discharge chamber and are shown by the shaded pattern in Fig. 5. The meshed surface is a stainless steel mesh laid on top of the discharge chamber surface near the optics end and is shown with a grid pattern in Fig. 5.

Other surface characteristics that had to be modeled were the perforated surfaces, which TRASYS was not designed to model. These surfaces are shown in Fig. 5 as dashed lines. Figure 6 shows a sampling of these surfaces. The plasma screen is located on the exterior of the thruster, and the accelerator and screen grids are part of the ion optics, with the outermost grid being the accelerator grid. To

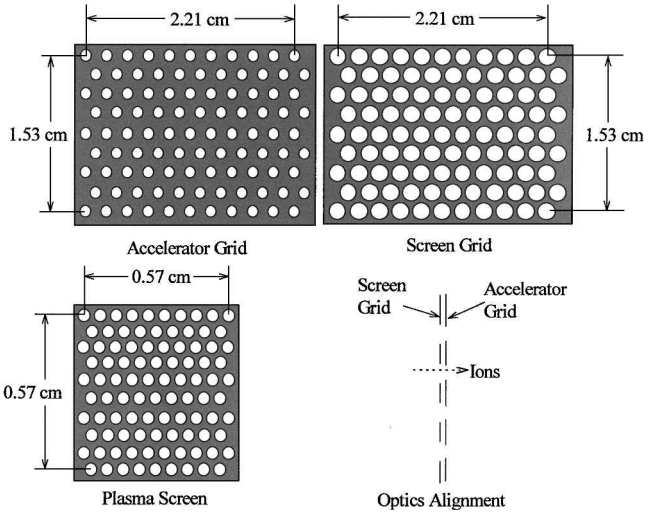

Fig. 6 Perforated surfaces on ion thruster.

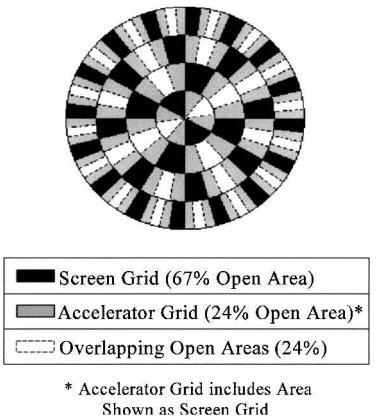

Fig. 7 Modeling approximation of ion optics used in TRASYS.

approximate these surfaces, transmissivity values were assigned to allow the appropriate percentage of incident energy to pass through all perforated surfaces. The value used for the transmissivity corresponded to the open area fraction of the perforated surface. However, it is not clear how accurate this assumption is for modeling these surfaces. For example, transmissive surfaces in series will artificially block radiation, which would normally travel through the aligned open areas of two perforated surfaces. Another approach in treating perforated surfaces is to model them as checkered surfaces. In this approach the amount of open area in the checkered surface corresponded to the same amount of open area present in the perforated surface. Figure 7 shows the checkered surface approximation used to model the grids. The screen grid is shown as black such that the nonblack area corresponds to the same amount of area in the actual screen grid, which is open. The accelerator grid is shown as gray, but also includes the area shown by the black screen grid. This then leaves the white area to be the open area, which is the same as the actual accelerator grid. This white area is also the aligned open area that allows the appropriate amount of interior thruster radiation to pass through the grids to the exterior without obstruction. The grids of the engine were modeled here both as transmissive surfaces and as coarse checkered surfaces, where coarse refers to the large checkered sections; fine would mean many small sections as opposed to few larger sections.

The accuracy of these various thermophysical properties in the model were established using comparisons between the model and cold-soak experiments with the nonoperating thruster in the shroud.

B. Self-Heating due to Plasma Interaction

One of the more complex aspects of the thruster model is ascertaining the amount of thruster self-heating from the plasma interaction with surfaces. To determine analytically the amount of heat that is produced by the plasma, several characteristics must be well understood. One of these characteristics is the precise location of the deposition of charged particles on the various surfaces. Other characteristics include the particle temperatures and the rate they are deposited on the surface in the discharge chamber.

The alternative used for this model entailed using previous heat-flux data from past work and then adjusting the values until the temperatures in the model agreed with the experimental data (Refs. 5, 6). However, the previous thrusters were somewhat different from the NSTAR thruster. The previous thrusters were not ring cusp thrusters with xenon propellant, but were divergent field thrusters using mercury propellant. This changes the thermal characteristics in several ways.

First, because the magnetic field is a ring cusp, the heating from the plasma will be in different locations. For example, Oglebay[6] and Wen et al.[5] report the power deposited in the front and back portion of the anode. However, the electrons will most likely be deposited differently because the two different types of thrusters have different magnetic field lines that the electrons follow.

Second, changing propellants also has a significant effect. The mercury-based thrusters had to have vaporizers to make sure the mercury was not in liquid form, but the xenon thrusters do not need these vaporizers. Xenon also has an ionization potential of 12.13 eV compared to mercury's 10.44 eV. This changes the amount of energy deposited when an ion recombines at a surface.

Third, the physical layout of the thrusters are also different. The NSTAR thruster has a conical rear portion, and the anode consists of the entire discharge chamber wall, whereas the other thrusters have an anode, which is not the entire wall, mounted to the engine body with gaps that cause heating of the engine body.

Because the thrusters have these various differences, values used from Oglebay[6] and Wen et al.[5] for the power deposited on the thruster are only rough starting points and would not be expected to give an accurate description of the NSTAR power deposition. However, they still would give a good starting point because there are enough similarities between thrusters and their operation. The initial estimate for power deposited on the NSTAR thruster was determined by considering only the components the previous thrusters had in common with the current thruster, the rest were disregarded. Then the values were interpolated or extrapolated from the previous thruster based on beam current, which is the current used by Oglebay[6] to scale. Table 2 gives the final values used by Wen et al.[5] and Ogelbay.[6] Several of the Wen et al. final heating values changed from 20 to 67% from their initial estimates.[5] Table 3 then contains the a priori and final heating power values used for the NSTAR thruster.

Table 2 Self-heating values used for Wen et al.[5] and Oglebay's[6] ion thrusters

	Wen et al.[5]		Oglebay[6]	
Description	0.5 A,[a] Power, W	1.0 A,[a] Power, W	1.0 A,[a] Power, W	1.9 A,[a] Power, W
Main vaporizer	——	——	7.3	7.3
Cathode vaporizer	——	——	4.6	7.6
Neutralizer vaporizer	——	——	3.0	4.9
Neutralizer tip	——	——	2.0	3.4
Cathode tip	12.6	15.4	13.4	25.6
Accelerator grid	10.1	11.8	11.6	19.6
Screen grid	5.9	11.6	11.6	19.6
Anode, rear	14.7	28.8	17.6	35.2
Anode, front	28.1	44.2	35.2	64.6
Engine body, rear	——	——	42.8	70.4
Engine body, front	——	——	9.2	15.6
Baseplate	16.1	36.7	36.8	46.8
Pole	9.9	18.2	14.4	24.0
Keeper baffle	11.2	20.6	——	——
Pole piece (side)	14.0	31.1	——	——
Housing	13.1	20.2	——	——
Total	135.7	238.6	209.5	344.6

[a]Beam current.

Table 3 A priori values based on Wen et al.[5] and Oglebay's[6] values and final adjusted values

		A priori values			Final values		
Nodes	Description	0.5 kW,[a] 0.56 A,[b] Power, W	1.3 kW,[a] 0.98 A,[b] Power, W	2.3 kW,[a] 1.75 A,[b] Power, W	0.5 kW,[a] 0.56 A,[b] Power, W	1.3 kW,[a] 0.98 A,[b] Power, W	2.3 kW,[a] 1.75 A,[b] Power, W
13	Cathode tip	7.4	13.8	23.6	11.5	15.0	22.5
201–204	Discharge chamber, rear	20.0	36.0	45.1	12.0	22.0	38.0
205–208	Anode, rear	10.0	28.0	32.3	44.0	42.0	50.0
209–212	Anode, middle	25.0	25.0	59.7	18.0	38.0	72.0
221–224	Anode front (near grids)	16.0	30.4	56.8	32.4	42.0	72.0
309	Screen grid	8.0	11.5	18.3	1.0	2.0	5.0
310	Accelerator grid	8.0	11.5	18.3	1.0	2.0	5.0
403	Neutralizer tip	1.3	2.0	3.2	31.0	28.0	28.0
501–504	Keeper	12.0	38.0	34.7	23.2	38.0	44.0
Total		107.7	196.2	292.0	174.1	229.0	336.5

[a]Throttling point. [b]Beam current.

Once the self-heating values were adjusted to correlate the temperatures between the model and the experiment, the total power of self-heating was compared to the analytically derived level. The total heat applied to the discharge chamber was determined analytically by taking the total power input to the system and subtracting out the neutralizer power and the power exiting in the ion beam. The following equation shows this energy balance:

$$\Phi_{\text{sh}} = \Phi_T - \Phi_N - J_B(V_P + U_+) \tag{4}$$

The thruster was modeled thermally for the power throttling levels of 0.5, 1.3, and 2.3 kW.

III. Results and Discussion

The computer model was first compared to the cold-soak test that was done at John H. Glenn Research Center. The temperatures for the boundary conditions in the model consisted of monitored shroud temperatures.

Figure 8 shows a cross-sectional view of the NSTAR thruster with the temperatures determined experimentally and by the SINDA computer model for the steady state case. Steady state was defined as when the temperature of the thruster was changing less than 3°C/h. Steady state was reached after about 10 h, and then reported values were taken at about 24 h after the beginning of the test.[11] The two temperatures derived from the computer model correspond to different approaches to modeling the optics (checkered vs transmissive). The SINDA model accurately predicted all thermocouple values within 5°C except at four nodes. Two of those four on the optics support ring are within 7°C. The other two, on the edge of the mask and front edge of the thruster, are within 10°C and are shown in Fig. 8 with the temperatures enclosed in a double-lined box.

The application of the model to the cold-soak experiment is necessary to determine the accuracy of the thermophysical properties of the thruster (radiative and conductive) independent of the plasma self-heating. It is difficult to determine the discrepancy of the temperatures in the mask area. This may reflect the difficulty in determining the contact resistance between the mask and the rest of the thruster.

The effect of changing the method of modeling the optics appears to be minimal in this case. Most of the temperatures changed by only a degree or two Celsius. The most drastic change in temperature was in the optics (2°C). This would indicate that modeling the surface as transmissive is sufficient for the conditions considered in the cold-soak test simulation.

The NSTAR thruster has also been modeled in SINDA to predict its transient behavior. The temperatures of the shroud, which were used as boundary conditions, are shown in Fig. 9. The experiment obtaining the transient values did not run to steady state and was performed prior to the experiment that was used for its steady-state values. The transient experiment did not have a door on the shroud, nor was there liquid nitrogen cooling the rear of the shroud, and it only used two thermocouples to measure shroud temperatures. These thermocouples were located on opposite sides of the shroud wall's circumference and about halfway from each

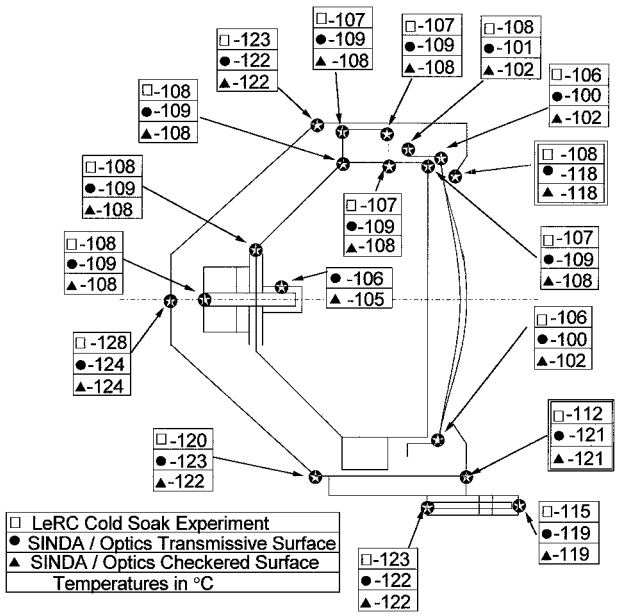

Fig. 8 NSTAR thruster steady-state temperatures under cold-soak conditions.

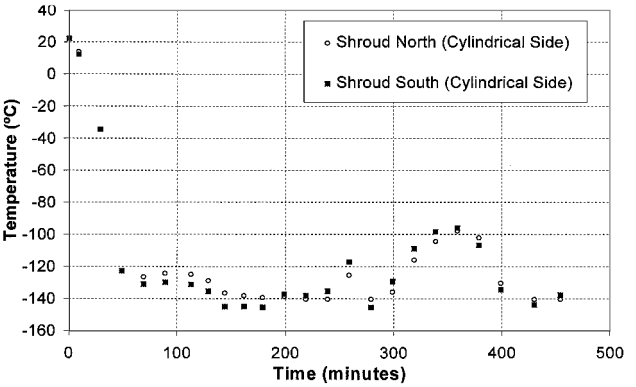

Fig. 9 Transient temperatures of shroud in cold-soak experiment.

end. Figures 10–12 show a comparison between experimentally determined data and the SINDA model with the optics modeled as transmissive surfaces.

The predicted results from SINDA agree to within 10°C for all of the nodes except nodes 112 (mask), 400 (neutralizer rear), and 102 and 104 (plasma screen). A major cause of the differences with the neutralizer temperatures is a result of the simple neutralizer model used. The areas of greatest discrepancy tend to be along the plasma screen and mask. Again, this may represent the difficulty in determining some of the contact resistances in the system and in

Table 4 Energy interchange between plasma screen, discharge chamber, and environment for the cold-soak experiment

	Transmissive optics				Checkered optics			
From node	To plasma screen, W	To discharge chamber, W	To shroud and tank, W	To shroud, %	To plasma screen, W	To discharge chamber, W	To shroud and tank, W	To shroud, %
101	——	0.011	0.267	96.0	——	0.011	0.268	96.1
102	——	0.051	0.234	82.1	——	0.055	0.235	81.0
104	——	0.011	0.200	94.8	——	0.012	0.201	94.4
108	——	0.008	0.283	97.3	——	0.009	0.285	96.9
112	——	0.0004	0.057	98.6	——	0.0005	0.058	99.1
203	0.003	——	0.042	93.3	0.003	——	0.047	94.0
207	0.005	——	0.088	94.6	0.006	——	0.099	94.3
211	0.004	——	0.039	90.7	0.004	——	0.049	92.5
215	0.004	——	0.035	89.7	0.004	——	0.036	90.0
219	0.005	——	0.030	85.7	0.005	——	0.030	85.7
223	0.001	——	0.022	95.7	0.001	——	0.030	96.8

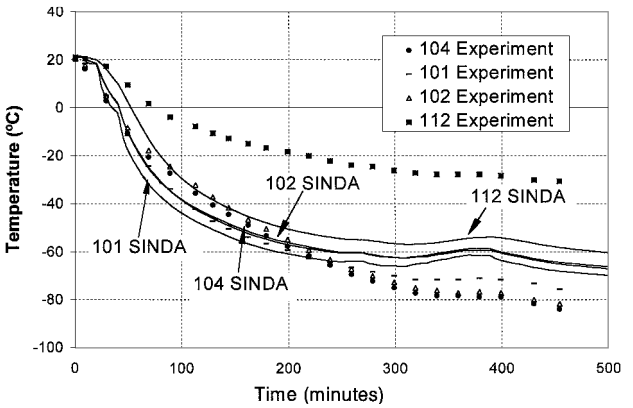

Fig. 10 Transient cold-soak experiment compared to SINDA model of NSTAR thruster for plasma screen nodes.

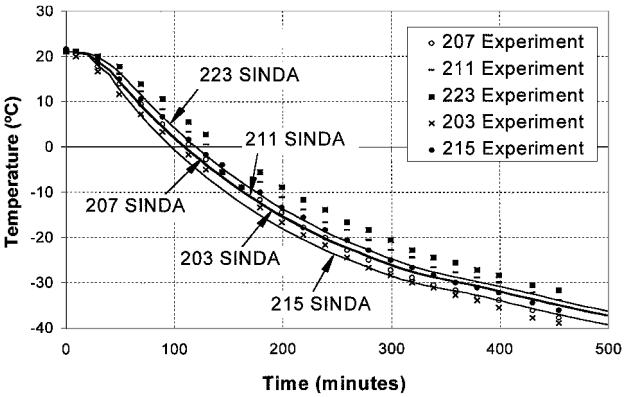

Fig. 11 Transient cold-soak experiment compared to SINDA model of NSTAR thruster for discharge chamber nodes.

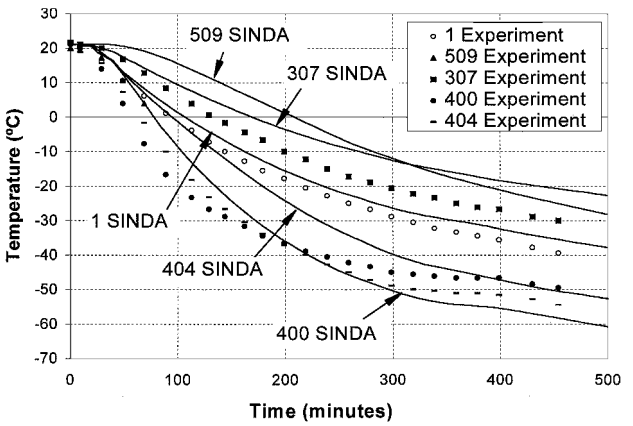

Fig. 12 Transient cold-soak experiment compared to SINDA model of NSTAR thruster.

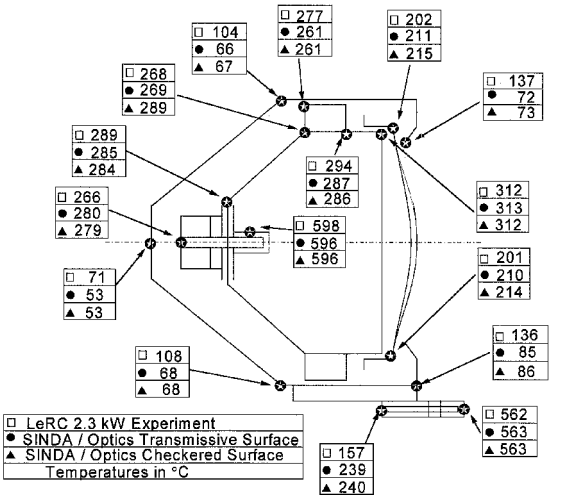

Fig. 13 NSTAR thruster steady-state temperatures when operating at 2.3 kW.

modeling perforated surfaces. In Fig. 10 the nodes corresponding to the plasma screen (Nodes 1xx) increase in temperature unexpectedly during 300 to 400 min. This is due to an increase in the shroud temperatures shown in Fig. 9. The modeled plasma screen surfaces in SINDA are more sensitive to the shroud temperatures than the actual plasma screen surfaces in the experiment. This sensitivity could be due to a difference in thermal capacitance between the modeled and the actual plasma screen surfaces, and it could also be affected by the method of modeling the perforated surface.

Figure 11 shows that the agreement of temperatures in the discharge chamber area is very good. The temperatures follow within 5°C throughout the test. The accuracy in the discharge chamber surface temperatures is crucial because most of the important components in the thruster are on or near this surface. The model also shows that the discharge chamber is interacting with its surroundings (the shroud) as in the experiment. The energy exchange between the plasma screen and the discharge chamber is of less influence than between the shroud and the discharge chamber because the plasma screen is perforated and, hence, only a portion of its surface interacts with the discharge chamber and because the emissivity of the screen (0.1) is considerably lower than that of the shroud (0.9). Table 4 shows this interaction for the cold-soak case. The energy exchange for both the plasma screen and the discharge chamber with the shroud is approximately an order of magnitude more than it is with each other. The energy exchange for the discharge chamber to the plasma screen and shroud is generally over 90% with the shroud. Thus, even though the temperatures of some outer components such as the plasma screen may be less accurate, as shown in Figs. 10 and 12, their impact on the discharge chamber is minimal.

The next step was to examine an operating thruster. Figures 13–15 give the temperatures on the NSTAR thruster when it was operating at the levels of 2.3, 1.3, and 0.5 kW, as well as the temperatures for

Table 5 Energy interchange between plasma screen, discharge chamber, and environment for the 2.3-kW throttling level

	Transmissive optics				Checkered optics			
From node	To plasma screen, W	To discharge chamber, W	To shroud and tank, W	To shroud, %	To plasma screen, W	To discharge chamber, W	To shroud and tank, W	To shroud, %
101	——	3.72	7.07	65.5	——	3.71	7.12	65.7
102	——	4.06	6.68	62.2	——	4.04	6.73	62.5
104	——	4.00	5.00	55.6	——	4.01	5.06	55.8
108	——	3.27	4.13	55.8	——	3.60	4.25	54.1
112	——	0.19	0.51	72.9	——	0.24	0.53	68.8
203	0.99	——	5.58	84.9	1.03	——	5.94	85.2
207	1.83	——	10.00	84.5	1.95	——	11.00	84.9
211	1.67	——	4.55	73.2	1.78	——	5.47	75.4
215	1.36	——	4.23	75.7	1.36	——	4.22	75.6
219	1.58	——	3.20	66.9	1.57	——	3.19	67.0
223	0.58	——	3.03	83.9	0.73	——	4.12	84.9

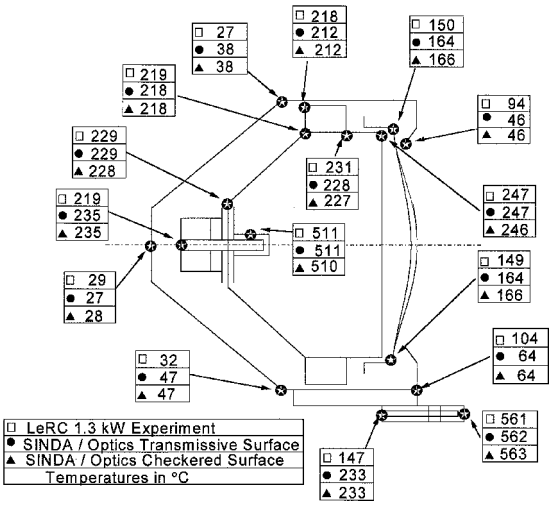

Fig. 14 NSTAR thruster steady-state temperatures when operating at 1.3 kW.

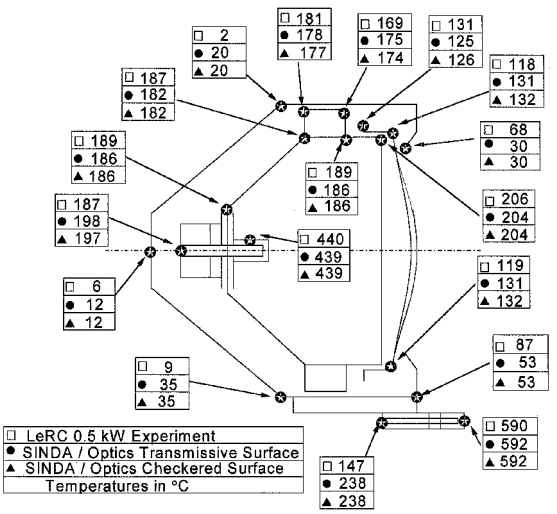

Fig. 15 NSTAR thruster steady-state temperatures when operating at 0.5 kW.

the SINDA model for both types of optic surface representations. Some of the thermocouples were not operating for some of the experiments, and so some of Figs. 13–15 will not have data for certain nodes.

As mentioned, prior initial values of self-heating were used and then adjusted to correspond to the experimental data. The temperatures of the discharge chamber were 30−40°C cooler than the experiment using the a priori self-heating values prior to adjusting. The self-heating values determined after adjusting are given in Table 3. After subtracting the power for the neutralizer, this method resulted in 308.5 W being applied to the thruster for the 2.3-kW throttling level, 201.0 W for the 1.3-kW throttling level, and 143.1 W for the 0.5-kW throttling point.

To verify this result, we use Eq. (4), where for the 2.3–kW throttling point $\Phi_T = 2274$ W, $\Phi_N = 23$ W, $J_B = 1.74$ A, $V_P = 1100$ V, and $U_+ = 12.13$ eV result in the applied heat being 316 W. The 308.5 W derived from the model is 2% of the calculated value. Evaluating the 1.3- kW throttling point, where $\Phi_T = 1305$ W, $\Phi_N = 28$ W, $J_B = 0.984$ A, $V_P = 1100$ V, and $U_+ = 12.13$ eV, gives the self-heating power as 182 W. The SINDA thermal model provided a value of 201.0 W, which is 10% larger. For the lowest throttling point of 0.5 kW, where $\Phi_T = 533$ W, $\Phi_N = 32$ W, $J_B = 0.56$ A, $V_P = 650$ V, and $U_+ = 12.13$ eV, Eq. (4) produces a self-heating power value of 130 W, which is about 10% lower than the 143.1-W value derived from the model. Both the model and the analytical values for the self-heating power show that the self-heating power to the spacecraft does not increase as rapidly as the throttling powers do. From the standpoint of thermal losses, this would indicate that the thruster is more efficient at higher power throttling points.

The temperatures of the anode in the discharge chamber are within 5°C of the experimental data for all of the throttling points except for node 211 in the 2.3-kW case, which is 7−8°C different. The nodes on the support ring (nodes 215 and 219) are within 6°C for the 0.5- and 1.3-kW throttling points; however, node 215 is 16°C different for the 2.3-kW case. The optics support is within 15°C for all throttling points. The base of the main cathode assembly is 10−16°C too warm for all cases. The plasma screen has some of the worst temperature fits varying from a few degrees different from experiment to 50°C different, and the mask is as much as 65°C cooler than experimentally determined. The base of the neutralizer is also rather different than experiment. However, the neutralizer was only included in very simple form because it was determined by Oglebay[6] to impact the thruster minimally. Its temperature correlation could be improved, but its temperature was not considered important for this analysis. The discrepancy of the plasma screen, mask, and optics assembly is most likely caused again by the difficulty in modeling a finely perforated surface and modeling contact resistances. The coupling between the discharge chamber and the plasma screen is through isolators that have a high number of contact points. Similar to the cold-soak case, the interaction between the discharge chamber and the environment is accurate. Table 5 shows the energy exchange between the plasma screen, discharge chamber, and shroud for the 2.3-kW case. The percent of energy exchange between the discharge chamber and the shroud is lower than in the cold-soak case, but still 67−85% of the energy exchange is with the shroud. The temperature of the plasma screen has a larger influence than in the cold-soak case, but it is still the outer environment that has a greatest impact on the discharge chamber. Therefore, this model will give an accurate prediction of the temperatures of the discharge chamber and its components under varying conditions. This is supported by the good agreement between the amount of self-heating energy supplied for the model and that derived analytically.

Once the model is calibrated, it can be used to predict various thruster operating scenarios. One of the major concerns is knowing

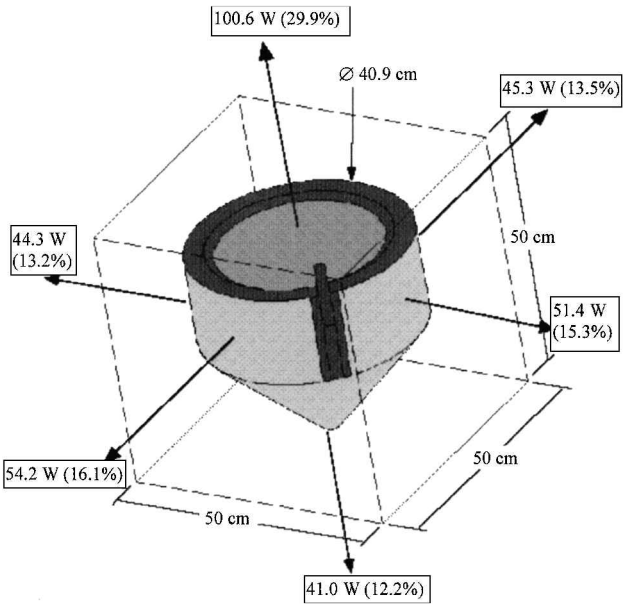

Fig. 16 Heat flux from NSTAR thruster to sides of a box with space conditions.

the direction heat is flowing out of the thruster and, in particular, the amount of heat that will be directed toward a spacecraft. To estimate the directional heat fluxes, the thruster was modeled in a box maintained at a temperature of −273°C and an emissivity of 1.0 (Fig. 16). The thruster was then given the heat distribution corresponding to the 2.3-kW throttle point.

It can be seen in Fig. 16 that a majority of the heat is expelled through the optics of the engine. It should be noted that the effect of the plasma is only included as the heat applied to thruster components, and the power through the grids does not include the ion beam power. The sides of the thruster are uniform in power distribution with a slight variation caused by the neutralizer, with the rear having the lowest amount of power lost thermally. However, these values would change if an object of different temperature were on any side of the thruster. If a large spacecraft surface was behind the thruster at a much higher temperature than absolute zero, the amount of heat flux in that direction would be drastically reduced. Thus, thermally, it appears that the thruster will have only a small impact on the spacecraft located behind it.

Because a majority of the heat transfer away from the thruster is through the optics, the direction the optics face will have the most effect on the thruster temperatures. If the thruster optics were facing the sun the thruster temperatures would be increased more than when facing other directions (assuming that the sun exposed areas were similar in dimensions). However, the thruster will be cooled the most when the optics are facing toward the cold of space. What the thruster optics will be facing will determine what the emissivity should be for the surface. If the thruster needs to be cooled and its optics are facing space, increasing the emissivity of the discharge chamber surface through a process such as grit blasting would be desired. However, if the thruster was going to be positioned with the optics toward the sun a majority of the time, it would be desired to have the inside of the discharge chamber as polished as possible to minimize solar heating.

IV. Conclusions

The developed SINDA thermal model accurately models the NSTAR thruster discharge chamber and components to within 10°C for several different throttling levels and conditions. There is a larger discrepancy with the temperatures on the plasma screen and mask. However, it has been shown that this has minimal effect on the temperatures of the discharge chamber and its components. There is still an accurate representation of the interaction between the inner surfaces and the environment. Changing the discharge chamber, whether by a material change or a change in its layout, will have the greatest effect on the thruster temperatures. The plasma screen and neutralizer were shown to be of lesser importance to the thruster thermal environment.

Limitations of the model include approximating perforated surfaces and modeling of contact resistance. There are no thermal tools currently available to model finely perforated surfaces. Not only is the determination of radiation view factors more difficult, calculating the conduction along the material is also more challenging. Some work has been done to further approximate the perforated surface. The methods used here included modeling the surface as having a transmissivity equal to the open area fraction and creating a coarse checkered pattern of appropriate open area. Whereas the dominant form of heat transfer is radiation, it was shown that contact resistance plays a significant role in the connection of the discharge chamber to the plasma screen via conduction. Currently, the best way to model contact resistance for a particular case is to estimate it using published data and then adjust the model at those points to the temperatures found experimentally.

The self-heating terms were developed from experimental data. Further work is being done to determine these terms analytically for various cases. The model is now capable of being integrated into various environments. It can be used to investigate spacecraft integration issues and evaluate proposed design changes from a thermal impact point of view.

Acknowledgments

This work was supported by a research grant from the John H. Glenn Research Center (NAG3-1572). James Sovey is the Contract Monitor. Thanks are given to Roger Myers and Frank Curran.

References

[1]Gatsonis, N. A., Samanta Roy, R. I., and Hastings, D. E., "Numerical Investigation of Ion Thruster Plume BackFlow," AIAA Paper 94-3140, June 1994.

[2]Polk, J. E., Anderson, J. R., Braphy, J. R., Rawlin, V. K., Patterson, M. J., Sovey, J. S., "The Effect of Engine Wear on Performance in the NSTAR 8000 Hour Ion Engine Endurance Test," AIAA Paper 97-3387, July 1997.

[3]Lide, D. R., *CRC Handbook of Chemistry and Physics,* 71st ed., CRC Press, Boca Raton, FL, 1990, pp. 4–37.

[4]MacRae, G. S., Zavesky, R. J., and Gooder, S. T., "Structural and Thermal Response of 30 cm Diameter Ion Thruster Optics," AIAA Paper 89-2719, July 1989.

[5]Wen, L., Crotty, J. D., and Pawlik, E. V., "Ion Thruster Thermal Characteristics and Performance," *Journal of Spacecraft and Rockets,* Vol. 10, No. 1, 1973, pp. 35–41.

[6]Oglebay, J. C., "Thermal Analytical Model of a 30 cm Engineering Model Mercury Ion Thruster," NASA TM X-71680, Jan. 1975.

[7]Cullimore, B. A., Goble, R. G., Jensen, C. L., and Ring, S. G., "Systems Improved Numerical Differencing Analyzer and Fluid Integrator; User's Manual," Contract NAS9-17448, Martin Marietta Corp., Denver, CO, March 1990; also NASA MCR-90-512, March 1990.

[8]Anderson, G. E., "Thermal Radiation Analyzer System (TRASYS); User's Manual," Contract NAS9-17900, Lockheed Engineering and Management Services Co., Houston, TX, April 1988, also NASA JSC-22964, April 1988.

[9]Gilmore, D. G., *Satellite Thermal Control Handbook,* The Aerospace Corp. Press, El Segundo, CA, 1994, pp. 3-14, 5-61–5-65.

[10]Keller, J. R., "Validation of the SINDA/FLUINT Code Using Several Analytical Solutions," *Sixth Annual Thermal and Fluids Analysis Workshop*, NASA CP 10161, Aug. 1994, pp. 69–84.

[11]Rawlin, V., Patterson, M., and Becker, R., "Thermal Environment Testing of NSTAR Engineering Model Ion Thrusters," *Proceedings of the 25th International Electric Propulsion Conference*, Paper 97-051, Cleveland, OH, Aug. 1997.

[12]Holman, J. P., *Heat Transfer*, 7th ed., McGraw–Hill, New York, 1990, pp. 666, 667.

[13]Incropera, F. P., and De Witt, D. P., *Fundamentals of Heat and Mass Transfer*, 3rd ed., Wiley, New York, 1990, pp. A27–A29.

[14]Stevens, P., "Engineering Support Request # 96171-PS," Jet Propulsion Lab., California Inst. of Technology, Pasadena, CA, Aug. 1996.